Editors' Suggestion | Featured in Physics

Subrecoil Clock-Transition Laser Cooling Enabling Shallow Optical Lattice Clocks

X. Zhang,[1,2] K. Beloy,[1] Y. S. Hassan,[1,2] W. F. McGrew,[1,2,*] C.-C. Chen,[1,2] J. L. Siegel,[1,2] T. Grogan,[1,2] and A. D. Ludlow[1,2,†]

[1]National Institute of Standards and Technology, 325 Broadway, Boulder, Colorado 80305, USA
[2]University of Colorado, Department of Physics, Boulder, Colorado 80309, USA

(Received 23 March 2022; accepted 19 July 2022; published 8 September 2022)

Laser cooling is a key ingredient for quantum control of atomic systems in a variety of settings. In divalent atoms, two-stage Doppler cooling is typically used to bring atoms to the μK regime. Here, we implement a pulsed radial cooling scheme using the ultranarrow $^1S_0$-$^3P_0$ clock transition in ytterbium to realize subrecoil temperatures, down to tens of nK. Together with sideband cooling along the one-dimensional lattice axis, we efficiently prepare atoms in shallow lattices at an energy of 6 lattice recoils. Under these conditions key limits on lattice clock accuracy and instability are reduced, opening the door to dramatic improvements. Furthermore, tunneling shifts in the shallow lattice do not compromise clock accuracy at the 10^{-19} level.

DOI: 10.1103/PhysRevLett.129.113202

Laser cooled and trapped ionic, atomic, and molecular systems have realized exceptional quantum control. As a result, these systems have been ideal for fundamental physics studies [1], explorations of many-body physics [2,3], quantum computation implementation [4,5], quantum information applications [6,7], and precision measurements [8,9]. Over recent decades, atoms with two valence electrons have attracted significant attention for their enhanced capability of quantum control. Notably, these atoms possess both a ground and metastable excited state with zero electronic angular momentum, offering quantum coherence on timescales of seconds or beyond.

These atomic structure features are prominently exploited in optical lattice clocks. Remarkable quantum coherence has been experimentally realized using the "clock" transition between these states, enabling unprecedented levels of frequency accuracy at the 10^{-18} fractional level [10,11]. As a result, these clocks can be used as a redefining anchor for the International System of Units [12], to test the variation of fundamental constants [13], to measure Earth's geopotential [14,15], and to search for dark matter [16–18]. But as the performance in these applications improves, new considerations require even greater levels of quantum control. This control begins with lower atomic temperatures to minimize trapping inhomogeneity and maximize coherence.

For divalent atoms like ytterbium, strontium, and mercury, Doppler cooling on the narrow intercombination $^1S_0$-$^3P_1$ transition typically affords atomic temperatures in the range of one to tens of μK [11,19–22]. Evaporative cooling has been used to attain sub-μK temperature and quantum degeneracy [23,24], but is precluded in many applications because of atom loss and very long evaporation time. Techniques for additional cooling of strongly confined atoms have recently been demonstrated, but these are generally limited to the resolved-sideband regime [21,25–28]. Many trapped systems operate outside this regime, including most optical lattice clocks that employ a 1D lattice for metrological benefits.

Here we realize greater levels of quantum control with subrecoil laser cooling on the doubly forbidden clock transition (natural linewidth ≈ 8 mHz) in ytterbium, reaching temperatures down to tens of nK. In so doing, we help to resolve several critical problems in optical lattice clocks. While confining atoms in a "magic wavelength" optical trap helps reject lowest-order light shifts on the clock transition, higher-order effects make complete elimination impossible [21,25,29]. Moreover, Raman scattering of optical lattice photons quenches the excited metastable state, limiting the desired quantum coherence [30,31]. Here, pulsed clock-transition cooling enables efficient loading of shallow lattices down to 6 $E_r \approx k_B \times 600$ nK ($E_r = h^2/2m\lambda_l^2$ is the lattice recoil energy, λ_l is the optical lattice wavelength, h is Planck's constant, m is the atomic mass of the ^{171}Yb isotope, and k_B is the Boltzmann constant). At these depths, lattice light shifts and $^3P_0$ excited state quenching are strongly suppressed, making systematic uncertainty at the 10^{-19} level or below feasible. The nK-regime temperatures enable one to resolve motional transitions from distinct lattice bands, allowing extra control. Strong intersite tunneling is observed in the form of Bloch oscillations at 6 E_r, inducing a minimal frequency shift. The pulsed clock-transition cooling demonstrated here can benefit neutral atom quantum computing architectures [24,32,33], where lower temperatures suppress thermal dephasing to improve entanglement fidelity

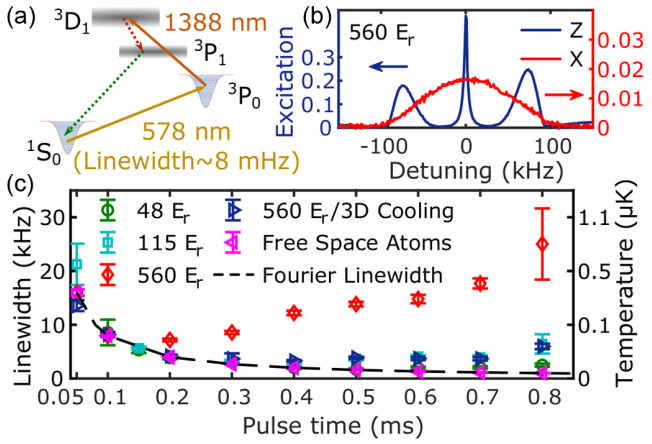

FIG. 1. (a) Energy levels used in the cooling. Note that spontaneous decay from $^3D_1$ (lifetime 330 ns [40]) follows the branching ratios 0.64 ($^3P_0$), 0.35 ($^3P_1$), and 0.01 ($^3P_2$, not shown). $^3P_1$ population decays to the ground state with a 870-ns lifetime [40]. (b) Atomic excitation as a function of laser detuning from the 578-nm transition for a laser propagating along the x (red) and z (blue) axes at 560-E_r lattice depth. (c) Measured linewidth of velocity selection profiles as a function of the first 578-nm laser pulse duration and for different trap depths [48 E_r (green circle), 115 E_r (cyan square), and 560 E_r (red diamond)] and cooling conditions [560 E_r after three-dimensional (3D) cooling (blue triangle)]. The magenta triangle data are measured with free-space atoms, and the black dashed line is the calculated Fourier-limited linewidth for different pulse durations. The right ordinate indicates the corresponding temperature of the selected atoms, from free-space Doppler theory.

and qubit control [28,34] or to enhance single-atom detection fidelity [35]. It also benefits strategies for direct cooling toward quantum degeneracy [36–38], as well as simulations of quantum magnetism, Kondo lattice physics [39], and other Hamiltonians [24,32].

Many details of our experimental apparatus are described elsewhere [10]. After Doppler cooling on the $^1S_0$-$^1P_1$ and $^1S_0$-$^3P_1$ transitions, atoms are loaded into a "magic wavelength" one-dimensional (1D) optical lattice at 759 nm. The lattice is formed using a power enhancement cavity with a $1/e$ field radius of 170 μm and aligned with $\leq 1°$ offset from gravity. We label this longitudinal axis z, and the radial axes x and y. One pair of counterpropagating, orthogonally polarized 578-nm laser beams (waist $= 400$ μm) travels along x, while a similar pair also travels along y. Both are used for selection in the pulsed clock-transition cooling. Another 578-nm laser propagates along $-z$ for longitudinal sideband cooling, while a final 578-nm laser propagates along $+z$ for narrow-line spectroscopy. A 1388-nm laser, resonant with the $^3P_0$-$^3D_1$ transition [Fig. 1(a)], travels with a small tilt relative to z and is used for both sideband cooling and pulsed radial cooling.

Atomic confinement along the radial and longitudinal axes differs significantly in our 1D lattice (strong confinement along z and weak confinement along x, y). To highlight this, Fig. 1(b) shows atomic excitation as a function of laser detuning from the $^1S_0$-$^3P_0$ transition at 578 nm for a laser propagating along the x or z axes. Along the z axis, strong confinement enables well-resolved (albeit motionally broadened) sidebands at red and blue detuning. For spectroscopy along x, weak confinement yields an excitation spectrum resembling the familiar Doppler-broadened profile, similar to the case of free-space atoms. The Doppler width is 118.4(12) kHz corresponding to a radial temperature of 17.4(4) μK.

Cooling along the radial axes begins by selectively exciting a velocity group within the Doppler-broadened distribution of Fig. 1(b) on the $^1S_0$-$^3P_0$ clock transition. We select two velocity groups by tailoring the counter-propagating 578-nm clock laser intensity, duration, and frequency detuning of the excitation pulse. Afterward, a pulse of 1388-nm laser light further excites the velocity-selected atoms in $^3P_0$ to $^3D_1$, where they spontaneously decay to $^1S_0$ via $^3P_1$, and the atomic velocity redistributes irreversibly through random recoil kicks (see the Supplemental Material [41]). By linking together a sequence of 578-nm and 1388-nm laser pulses, the atomic population accumulates in the zero-velocity dark state, which is off-resonance relative to the 578-nm velocity selection laser frequencies employed.

While the cooling principle is related to pulsed Raman cooling [42,43], here we exploit the ultranarrow clock transition for precise single-photon velocity selection, rather than a two-photon Raman process. The coherence of the long-lived $^3P_0$ state facilitates subrecoil temperatures. A related technique has also been used to 1D cool ^{40}Ca atoms in free space using the intercombination $^1S_0$-$^3P_1$ transition [44–46]. Here, atomic confinement not only enables repetitive and long-duration cooling pulses without atom escape, but the magic wavelength operation also prevents inhomogeneous trap light shifts from degrading the velocity selection.

However, the trap does introduce a challenge to the velocity selection process. Oscillatory atomic motion along the weak trap axes yields a periodic Doppler shift on the clock transition, broadening the velocity selection profile. To explore this effect experimentally, we excite trapped atoms near zero velocity with a resonant 578-nm laser π pulse along x. After removing any residual ground state atoms via repeated cycling on the $^1S_0$-$^1P_1$ transition at 399 nm, we use a second, longer-duration 578-nm π pulse along x with variable detuning to de-excite selected $^3P_0$ atoms back to the ground state, where 399-nm laser fluorescence measurements are made. To ensure that lattice confinement does not impact the de-excitation process, the lattice is abruptly extinguished prior to this second 578-nm pulse. The velocity selection profile is read out as detuning of the second pulse is scanned [see the Supplemental Material, Figs. 2(b) and 2(c) [41]].

Figure 1(c) shows the measured linewidth of the resulting velocity selection profiles, plotted as a function of the

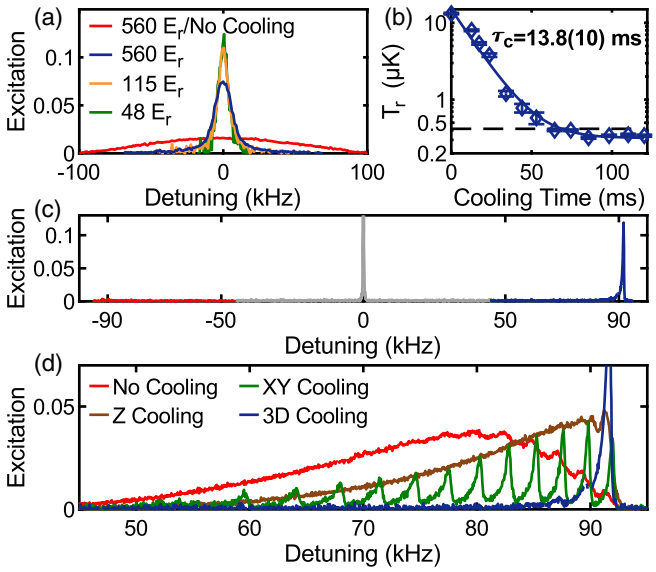

FIG. 2. (a) Radial spectra before (red) and after (blue) pulsed radial cooling at 560 E_r. The same cooling process was also realized at 48 E_r (green) and 115 E_r (orange). The corresponding radial temperatures of atoms are 17.4(4) μK, 250(10) nK, 90(10) nK, and 90(10) nK, respectively. The total cooling time for each trap depth is 84 ms, 93 ms, and 96 ms, respectively. Temperature is derived from the width of a Voigt line shape fit [41]. (b) Measured radial temperature as a function of cooling time at 560 E_r. The cooling time is adjusted by varying the number of pulse cycles applied. The solid line is the exponential fit. The black dashed line is the recoil-limited temperature of 410 nK. (c) Longitudinal sideband spectra at 560 E_r after 3D cooling. Red sideband, carrier, and blue sideband transitions are highlighted with the red, gray, and blue line, respectively. (d) Blue sidebands at 560 E_r under conditions of no clock-transition cooling (red), longitudinal sideband cooling alone (z cooling, brown), radial cooling alone (xy cooling, green), and 3D cooling (blue). In the green trace, we resolve transitions from different longitudinal lattice bands, whose frequency splitting is given by the trap anharmonicity.

first 578-nm laser pulse duration. Data for the reference case of free-space atoms, measured by releasing the atoms from the lattice before the first pulse, closely follows the Fourier limited width (dashed line). Red diamonds show the case of atoms in a deep lattice (560 E_r). At pulse durations above 0.2 ms, spectral profiles are significantly broadened from modulation effects in the trap. Measured and simulated Rabi flopping from radial excitation also highlights the effect (see the Supplemental Material [41]). After introducing additional cooling, or utilizing lower lattice depths (which also exhibit lower initial temperatures), the measured linewidths lie closer to the Fourier limit. To summarize, radial atomic motion in the lattice limits the narrow velocity selectivity afforded by the 578-nm pulse, but the degradation is reduced as the atoms are more deeply cooled.

During radial cooling, both x and y 578-nm lasers are pulsed on at the same time, followed by a 1388-nm laser (1 mW, 20-μs pulse duration) to bring the population back to the ground state. The 578-nm laser π pulses are tailored in duration and detuning to optimize the velocity selection, with pulses becoming longer and detuning smaller as the atoms get colder. The cooling pulse sequence, optimized for a lattice depth of 560 E_r, is shown in the Supplemental Material [41]. We observe better results by cycling one pulse many times, then moving forward to the next pulse parameters, rather than repeating a sequence of each tailored pulse multiple times. As shown in Fig. 2(a), cooling reduces the linewidth of the radial spectrum from 118.4(12) kHz to 14.2(2) kHz, corresponding to a temperature decrease of nearly 2 orders of magnitude from 17.4(4) μK to 250(10) nK. The cooled temperature represents a thermal energy equal to 0.4(1)% of the trap depth. The cooled radial temperature lies below the recoil limit of 410 nK, given by cascaded spontaneous decay $^3D_1$-$^3P_1$-$^1S_0$, shown as the dashed line in Fig. 2(b). Nevertheless, the velocity selection linewidth measurements in Fig. 1(c) suggest that temperatures below 100 nK should be possible. As has been observed in Raman cooling, side lobes in the excitation spectrum may degrade the dark state, and Blackman pulses could offer lower temperatures at the cost of increased cooling time [42]. Figure 2(b) shows the measured temperature versus cooling time, yielding a time constant of 13.8(10) ms. The possibility of fast cooling is beneficial to lattice clocks, to minimize the Dick effect [47]. We also cooled samples at lattice depths of 48 E_r and 115 E_r, reaching colder temperatures at 90(10) nK. We note that the pumping process at 1388 nm leads to 2.6% decay to the long-lived $^3P_2$ state per cycle. With many repeated cooling cycles, we observe as much as 75% population loss at 560 E_r. The addition of another laser to optically pump the population out of $^3P_2$ could eliminate the loss.

By combining pulsed radial cooling with longitudinal sideband cooling [25,26,41], atomic samples are cooled in all three dimensions. After cooling in one dimension, we typically observe residual heating in other dimensions. We therefore interleave sideband cooling with pulsed radial cooling. Figure 2(c) shows longitudinal sideband spectra at 560 E_r after 3D cooling. The red sideband is virtually gone since the atomic population resides in the ground lattice band. In Fig. 2(d), we show blue-detuned sidebands at 560 E_r under four different cooling situations. With no clock-transition cooling, the sideband exhibits a broad structure. After the application of pulsed radial cooling alone, distinct longitudinal lattice band transitions are well resolved, permitting measurement of the atomic distribution across the bands. On the other hand, after longitudinal sideband cooling alone, atoms occupy the longitudinal ground motional band, and the long tail of the sideband is due entirely to radial temperature. Finally, after 3D cooling, the width of the remaining sideband is dramatically narrowed, with virtually all population in the ground lattice band and cooled radially below the recoil limit.

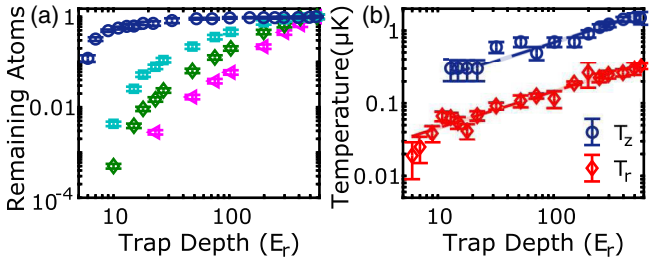

FIG. 3. (a) Remaining atomic fraction after adiabatically ramping to the indicated trap depth from 560 E_r after 3D cooling at 560 E_r (blue circle), after longitudinal sideband cooling alone (cyan square), or with no clock transition cooling at all (green diamond). Also included is the case of direct loading to a fixed lattice of indicated trap depth with no adiabatic ramp (magenta triangle). (b) Longitudinal temperature (T_z, blue circle) and radial temperature (T_r, red diamond) after adiabatically ramping to the indicated trap depth from 560 E_r after 3D cooling at 560 E_r. The dashed lines are fit with the expected adiabatic scaling.

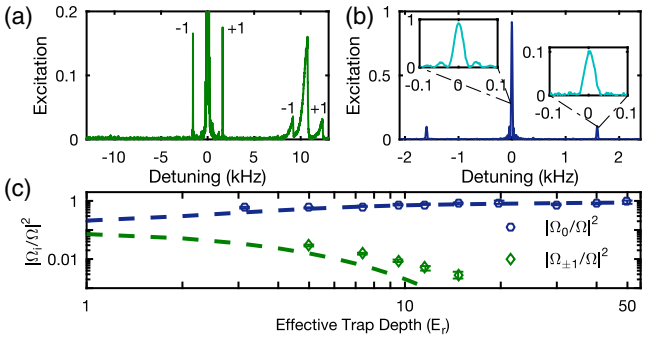

FIG. 4. (a) Longitudinal sideband and Bloch oscillation spectrum at 12 E_r. First-order Bloch oscillations (±1) are observed not only around the carrier transition but also around the blue sideband. (b) 30-ms π pulse Rabi spectroscopy at 6 E_r. Insets: enlarged views of the carrier spectrum and the first-order Bloch oscillation spectrum. (c) Measured relative Rabi frequencies of the carrier and the first-order Bloch oscillation transition as a function of trap depth. Dashed lines are theoretical calculations.

Armed with efficient 3D cooling on the clock transition, we load large atom numbers into a deep magic-wavelength lattice and then adiabatically ramp to shallow depths. The blue circles in Fig. 3(a) show the remaining population at the final trap depth, normalized to the initial population at 560 E_r. The majority of the population is preserved at depths $\leq 10\ E_r \approx k_B \times 1\ \mu$K. In absolute terms, we load thousands of atoms into a 6-E_r trap, which in this case is the lowest trap depth we can reach due to lattice tilt away from gravity. Figure 3(a) offers a comparison to cases with no cooling or longitudinal sideband cooling alone prior to the adiabatic ramp. Furthermore, the magenta triangles give the case of direct loading to a fixed lattice of indicated depth (with no adiabatic ramp). Ensuring that shallow lattices support high atom numbers is important for reaching excellent clock stability from quantum projection noise (QPN) [48]. Using short duration $\pi/2$ excitation pulses, we measured shot-to-shot fluctuations in the atomic excitation to assess our detection signal-to-noise ratio (SNR). With atom numbers from $N = 100$ to $N = 2 \times 10^4$, we observe an SNR scaling as $1/\sqrt{N}$, as expected for QPN. For the 1 Hz spectral linewidth with which we typically operate the lattice clock, this corresponds to an atomic detection-limited clock stability of $1.4 \times 10^{-17}/\sqrt{\tau}$ for averaging time τ in seconds.

We measure atomic temperature spectroscopically after adiabatic ramping, with longitudinal sideband spectra for longitudinal temperatures [49] and Doppler-broadened radial spectra for radial temperatures [41]. As shown in Fig. 3(b), the results follow the expected adiabatic scaling $1/\sqrt{U}$ (for trap depth U). At 6 E_r, the radial temperature is as low as 20 nK. For trap depths $\leq 10\ E_r$, no longitudinal temperature is plotted, since only the ground lattice band is trapped and motional sidebands are no longer present.

We consider the immediate benefits of 3D cooling for lattice clock operation. In our systematic uncertainty evaluation of two Yb lattice clocks at the 1.4×10^{-18} fractional frequency level [10], a dominant systematic uncertainty contributor stemmed from lattice light shifts. By operating with a lattice depth of 6 E_r as shown here, together with an improved characterization of polarizability from magnetic dipole and electric quadrupole couplings, lattice light shifts uncertainty can be reduced to the 1×10^{-19} level. With more precise measurement of the magic wavelength, even lower uncertainties are possible. Furthermore, based on measurements of lattice-induced $^3P_0$ quenching [50,51], the quenching rate at 6 E_r is more than 1 order of magnitude smaller than the spontaneous decay rate, yielding negligible impact on clock stability for interrogation times up to the clock state's natural lifetime [41]. Finally, ultracold atomic samples suppress p-wave inelastic losses that degrade spectroscopic contrast on the clock transition [31].

A potential drawback of shallow lattices is the increased intersite tunneling that can lead to motional frequency shifts during laser interrogation [52]. A typical strategy to mitigate these effects is to use the Wannier-Stark lattice, which aligns the optical lattice along gravity. Gravity lifts the energy degeneracy between adjacent lattice sites, inducing atomic localization via periodic Bloch oscillations [53]. We observe prominent Bloch oscillations for the shallowest lattices used here. Figure 4(a) shows a longitudinal sideband spectrum at a 12-E_r lattice depth. We observe first-order Bloch oscillation sidebands at $\Delta_g/2\pi = mg\lambda_l/2h \approx 1593$ Hz (where g is the local gravitational acceleration) around the carrier at zero detuning, as well as Bloch sidebands around the blue motional sideband near 10 kHz (indicating combined motional excitation and tunneling). Figure 4(b) displays the Bloch sideband spectrum for a 6-E_r lattice when excited by a 30-ms carrier π pulse, yielding 91% carrier excitation and 10% excitation

of the first-order Bloch sideband. In Fig. 4(c), we use measured excitation to deduce the relative Rabi frequencies $|\Omega_0/\Omega|^2$ and $|\Omega_{\pm 1}/\Omega|^2$ as a function of trap depth, where Ω_0, $\Omega_{\pm 1}$, and Ω are the Rabi frequencies of the carrier transition, the first-order Bloch oscillation transition, and an atom in free space, respectively. Dashed lines give a theoretical calculation based on overlap integrals of the Wannier-Stark wave functions [41] for atoms with finite radial temperature and accounting for radial gravitational sag due to slight lattice tilt with respect to gravity.

In the presence of Bloch oscillations, tunneling leads to frequency broadening and shifts on the order of $\Omega_{\pm 1}\Omega_0/\Delta_g$ [52]. While the average tunneling shift depends on the relative phase of the atoms across different lattice sites, for our typical 560-ms Rabi spectroscopy, the maximum effect can only be 10^{-19} level. Therefore, these shallow lattices can support substantially improved clock accuracy in the future.

Very recent work in strontium [54] highlights another potential complication of shallow lattices: s-wave atomic collision shifts mediated by tunneling. While more experimental investigation could be useful, we note that this effect is less relevant for ^{171}Yb, where tunneling in a Wannier-Stark lattice is more strongly suppressed by atomic mass.

In conclusion, we demonstrate a pulsed cooling scheme achieving radial atomic temperature in a 1D lattice in the nK regime, below the recoil limit. Combined with longitudinal sideband cooling, we realize fast ultracold temperatures in all three dimensions, allowing for the efficient transfer of atoms to a shallow lattice, where lattice light shifts and $^3P_0$ excited state quenching are strongly suppressed. Finally, we observe Bloch oscillations over a range of trap depths with tunneling shifts bounded at the low 10^{-19} level. This Letter paves the way for next-generation lattice clock uncertainty and stability, as well as enhanced control in quantum computation and simulation experiments [41].

We appreciate experimental assistance from R. Brown, C. Oates, and D. Nicolodi, as well as R. Brown and C. Oates for careful reading of the manuscript. This work was supported by NIST, ONR, and NSF QLCI Award No. 2016244.

*Present address: JILA, University of Colorado and National Institute of Standards and Technology, Boulder, Colorado 80309, USA.

†andrew.ludlow@nist.gov

[1] M. S. Safronova, D. Budker, D. DeMille, Derek F. Jackson Kimball, A. Derevianko, and C. W. Clark, Rev. Mod. Phys. **90**, 025008 (2018).

[2] I. Bloch, J.Dalibard, and W. Zwerger, Rev. Mod. Phys. **80**, 885 (2008).

[3] B. Yan, S. A. Moses, B. Gadway, J. P. Covey, K. R. A. Hazzard, A. M. Rey, D. S. Jin, and J. Ye, Nature (London) **501**, 521 (2013).

[4] D. Jaksch, H. J. Briegel, J. I. Cirac, C. W. Gardiner, and P. Zoller, Phys. Rev. Lett. **82**, 1975 (1999).

[5] D. DeMille, Phys. Rev. Lett. **88**, 067901 (2002).

[6] H. Bernien, S. Schwartz, A. Keesling, H. Levine, A. Omran, H. Pichler, S. Choi, A. S. Zibrov, M. Endres, M. Greiner, V. Vuletić, and M. D. Lukin, Nature (London) **551**, 579 (2017).

[7] J. W. Park, Z. Z. Yan, H. Loh, S. A. Will, and M. W. Zwierlein, Science **357**, 372 (2017).

[8] A. D. Ludlow, M. M. Boyd, J. Ye, E. Peik, and P. O. Schmidt, Rev. Mod. Phys. **87**, 637 (2015).

[9] W. B. Cairncross, D. N. Gresh, M. Grau, K. C. Cossel, T. S. Roussy, Y. Ni, Y. Zhou, J. Ye, and E. A. Cornell, Phys. Rev. Lett. **119**, 153001 (2017).

[10] W. F. McGrew, X. Zhang, R. J. Fasano, S. A. Schäffer, K. Beloy, D. Nicolodi, R. C. Brown, N. Hinkley, G. Milani, M. Schioppo, T. H. Yoon, and A. D. Ludlow, Nature (London) **564**, 87 (2018).

[11] T. Bothwell, D. Kedar, E. Oelker, J. M. Robinson, S. L. Bromley, W. L. Tew, J. Ye, and C. J. Kennedy, Metrologia **56**, 065004 (2019).

[12] F. Riehle, P. Gill, F. Arias, and L. Robertsson, Metrologia **55**, 188 (2018).

[13] R. Lange, N. Huntemann, J. M. Rahm, C. Sanner, H. Shao, B. Lipphardt, C. Tamm, S. Weyers, and E. Peik, Phys. Rev. Lett. **126**, 011102 (2021).

[14] T. E. Mehlstäubler, G. Grosche, C. Lisdat, P. O. Schmidt, and H. Denker, Rep. Prog. Phys. **81**, 064401 (2018).

[15] M. Takamoto, I. Ushijima, N. Ohmae, T. Yahagi, K. Kokado, H. Shinkai, and H. Katori, Nat. Photonics **14**, 411 (2020).

[16] P. Wcisło *et al.*, Sci. Adv. **4**, eaau4869 (2018).

[17] B. M. Roberts, P. Delva, A. Al-Masoudi, A. Amy-Klein *et al.*, New J. Phys. **22**, 093010 (2020).

[18] B. A. C. O. N. Collaboration, K. Beloy *et al.*, Nature (London) **591**, 564 (2021).

[19] N. D. Lemke, A. D. Ludlow, Z. W. Barber, T. M. Fortier, S. A. Diddams, Y. Jiang, S. R. Jefferts, T. P. Heavner, T. E. Parker, and C. W. Oates, Phys. Rev. Lett. **103**, 063001 (2009).

[20] S. Falke, N. Lemke, C. Grebing, B. Lipphardt, S. Weyers, V. Gerginov, N. Huntemann, C. Hagemann, A. Al-Masoudi, S. Häfner, S. Vogt, U. Sterr, and C. Lisdat, New J. Phys. **16**, 073023 (2014).

[21] I. Ushijima, M. Takamoto, and H. Katori, Phys. Rev. Lett. **121**, 263202 (2018).

[22] M. Pizzocaro, F. Bregolin, P. Barbieri, B. Rauf, F. Levi, and D. Calonico, Metrologia **57**, 035007 (2020).

[23] S. L. Campbell, R. B. Hutson, G. E. Marti, A. Goban, N. D. Oppong, R. L. McNally, L. Sonderhouse, J. M. Robinson, W. Zhang, B. J. Bloom, and J. Ye, Science **358**, 90 (2017).

[24] F. Schäfer, T. Fukuhara, S. Sugawa, Y. Takasu, and Y. Takahashi, Nat. Rev. Phys. **2**, 411 (2020).

[25] R. C. Brown, N. B. Phillips, K. Beloy, W. F. McGrew, M. Schioppo, R. J. Fasano, G. Milani, X. Zhang, N. Hinkley, H. Leopardi, T. H. Yoon, D. Nicolodi, T. M. Fortier, and A. D. Ludlow, Phys. Rev. Lett. **119**, 253001 (2017).

[26] N. Nemitz, T. Ohkubo, M. Takamoto, I. Ushijima, M. Das, N. Ohmae, and H. Katori, Nat. Photonics **10**, 258 (2016).
[27] T. Bothwell, C. J. Kennedy, A. Aeppli, D. Kedar, J. M. Robinson, E. Oelker, A. Staron, and J. Ye, Nature (London) **602**, 420 (2022).
[28] A. Jenkins, J. W. Lis, A. Senoo, W. F. McGrew, and A. M. Kaufman, Phys. Rev. X **12**, 021027 (2022).
[29] N. Nemitz, A. A. Jørgensen, R. Yanagimoto, F. Bregolin, and H. Katori, Phys. Rev. A **99**, 033424 (2019).
[30] S. Dörscher, R. Schwarz, A. Al-Masoudi, S. Falke, U. Sterr, and C. Lisdat, Phys. Rev. A **97**, 063419 (2018).
[31] R. B. Hutson, A. Goban, G. E. Marti, L. Sonderhouse, C. Sanner, and J. Ye, Phys. Rev. Lett. **123**, 123401 (2019).
[32] A. J. Daley, Quantum Inf. Process. **10**, 865 (2011).
[33] G. Pagano, F. Scazza, and M. Foss-Geig, Adv. Quantum Technol. **2**, 1800067 (2019).
[34] I. S. Madjarov, J. P. Covey, A. L. Shaw, J. Choi, A. Kale, A. Cooper, H. Pichler, V. Schkolnik, J. R. Williams, and M. Endres, Nat. Phys. **16**, 857 (2020).
[35] J. P. Covey, I. S. Madjarov, A. Cooper, and M. Endres, Phys. Rev. Lett. **122**, 173201 (2019).
[36] S. Stellmer, B. Pasquiou, R. Grimm, and F. Schreck, Phys. Rev. Lett. **110**, 263003 (2013).
[37] J. Hu, A. Urvoy, Z. Vendeiro, V. Crépel, W. Chen, and V. Vuletić, Science **358**, 1078 (2017).
[38] A. Urvoy, Z. Vendeiro, J. Ramette, A. Adiyatullin, and V. Vuletić, Phys. Rev. Lett. **122**, 203202 (2019).
[39] M. Foss-Feig, M. Hermele, and A. M. Rey, Phys. Rev. A **81**, 051603(R) (2010).
[40] K. Beloy, J. A. Sherman, N. D. Lemke, N. Hinkley, C. W. Oates, and A. D. Ludlow, Phys. Rev. A **86**, 051404(R) (2012).
[41] See Supplemental Material at http://link.aps.org/supplemental/10.1103/PhysRevLett.129.113202 for additional details, including specification of the cooling sequence parameters.
[42] M. Kasevich and S. Chu, Phys. Rev. Lett. **69**, 1741 (1992).
[43] N. Davidson, H. J. Lee, M. Kasevich, and S. Chu, Phys. Rev. Lett. **72**, 3158 (1994).
[44] E. A. Curtis, C. W. Oates, and L. Hollberg, Phys. Rev. A **64**, 031403(R) (2001).
[45] T. Binnewies, G. Wilpers, U. Sterr, F. Riehle, J. Helmcke, T. E. Mehlstäubler, E. M. Rasel, and W. Ertmer, Phys. Rev. Lett. **87**, 123002 (2001).
[46] U. Sterr, T. Binnewies, C. Degenhardt, G. Wilpers, J. Helmcke, and F. Riehle, J. Opt. Soc. Am. B **20**, 985 (2003).
[47] G. J. Dick, In *Proc. Precise Time and Time Interval Meeting*, edited by R. L. Sydnor (US Naval Observatory, 1987), pp. 133–147.
[48] W. M. Itano, J. C. Bergquist, J. J. Bollinger, J. M. Gilligan, D. J. Heinzen, F. L. Moore, M. G. Raizen, and D. J. Wineland, Phys. Rev. A **47**, 3554 (1993).
[49] S. Blatt, J. W. Thomsen, G. K. Campbell, A. D. Ludlow, M. D. Swallows, M. J. Martin, M. M. Boyd, and J. Ye, Phys. Rev. A **80**, 052703 (2009).
[50] W. F. McGrew, Ph.D. thesis, University of Colorado Boulder, 2020.
[51] J. Siegel *et al.* (to be published).
[52] P. Lemonde and P. Wolf, Phys. Rev. A **72**, 033409 (2005).
[53] F. Bloch, Z. Phys. **52**, 555 (1929).
[54] A. Aeppli, A. Chu, T. Bothwell, C. J. Kennedy, D. Kedar, P. He, A. M. Rey, and J. Ye, arXiv:2201.05909.